Nonequilibrium Green's Function Modeling of Trap-Assisted Tunneling in In$_x$Ga$_{1-x}$N/GaN Light-Emitting Diodes

Jesus Alberto Gonzalez Montoya[1], Alberto Tibaldi[1,2,*], Carlo De Santi[3], Matteo Meneghini[3], Michele Goano[1,2] and Francesco Bertazzi[1,2]

[1] *DET, Politecnico di Torino, Torino, Italy*
[2] *IEIIT-CNR, Torino, Italy*
[3] *Department of Information Engineering, University of Padova, Italy*

This work presents an investigation of carrier transport in GaN-based light-emitting diodes in the subthreshold forward-bias regime where tunneling processes are relevant. A quantum kinetic theory of trap-assisted tunneling is developed within the framework of the nonequilibrium Green's function formalism. Based on fully nonlocal scattering self-energies computed in the self-consistent Born approximation and a multiband description of the electronic structure, the model provides access to spectral quantities, such as the local density of states and the current density, which are essential to understand the nature of the tunneling process. The quantum nonradiative recombination rates can be reproduced by the conventional Shockley-Read-Hall theory, provided that the classical charge is replaced with the correct quantum charge, which means that trap-assisted tunneling can be described with drift-diffusion solvers complemented with appropriate quantum corrections for the calculation of the local density of states. The subthreshold I-V characteristics and ideality factors predicted by the quantum kinetic model are in agreement with measurements.

I. INTRODUCTION

The presence of defects in GaN-based light-emitting diodes (LEDs) has often been correlated to the efficiency droop, the decline of the internal quantum efficiency at high current levels [1,2]. Among notable examples of defect-related droop theories is the density-activated defect recombination model proposed in Ref. [3], which assumes that at high injection levels, carriers spill from low-potential states localized near indium-rich clusters, reaching strong recombination centers in the high-potential regions. Experimental studies of recombination processes in high-quality III-nitride emitters suggested a wealth of physical effects beyond the commonly considered ABC model, e.g., alloy- and trap-assisted Auger transitions with lower energy threshold, which may possibly contribute to droop at high injection levels [4–6].

But the role of defects is probably more evident at low current densities. Below the optical turn on, before the radiative recombination sets in, traps may assist the tunneling of carriers, opening additional current leakage channels that would not be accessible by coherent band-to-band tunneling (BTBT). Indeed, the high ideality factors experimentally observed in the subthreshold I-V characteristics

of GaN-based LEDs is considered the signature of trap-assisted tunneling (TAT) [7–10]. Therefore, TAT is a sensitive indicator of the presence of defects, device growth quality, and degradation due to accelerated stress [11].

Within the drift-diffusion (DD) approximation, TAT is usually described by means of a conventional Shockley-Read-Hall (SRH) recombination model with electric-field-dependent carrier lifetimes, which account for the increase in carrier capture and emission rates due to possible tunneling from or to the trap state [12–14]. However, the so-called field enhancement factors are not just local functions of the electric field; in particular, near heterojunctions, they critically depend on the local density of states that participates in the tunneling process [15]. Of particular importance are the tail states that split from the corresponding bands into the gap, extending the voltage range of BTBT beyond the value where the alignment of the sharp band edges vanishes. Tail states may result from carrier-phonon and carrier-carrier interactions [16], confinement effects (bound states leaking in the barriers), or simply the band bending induced by built-in and/or applied electric fields.

In this work, we investigate TAT with a rigorous quantum transport approach based on the nonequilibrium Green's function (NEGF) formalism. The effective mass approximation usually employed in drift-diffusion

---
*alberto.tibaldi@polito.it

calculations is not appropriate for the valence band, due to band anisotropy, and the mixing of heavy- and light-hole states. The local density of states (LDOS) is clearly one of the critical ingredients for the calculation of TAT [15, 17]. Therefore, a multiband $k \cdot p$ envelope-function model is adopted for an accurate description of the electronic structure. In order to include the possible contribution of phonon processes in the determination of the LDOS, the coupling to acoustic and polar optical phonons is considered within the deformation potential and the Fröhlich formalism, respectively, by means of fully nonlocal self-energies computed in the self-consistent Born approximation. We neglect carrier-photon interactions, since this study is limited to the subthreshold regime, below the optical turn on. Following Ref. [18], an additional self-energy is included to describe the multiphonon probability for nonradiative transitions.

TAT can be either seen as a thermal capture or emission of carriers enhanced by the field, which leads to the picture of a field-assisted recombination process (i.e., the concept of field-enhancement factors), or as a tunneling process assisted by multiphonon defect recombination [14]. This distinction is not needed within the NEGF formalism, as self-energies and Green's functions are determined self-consistently. Thus, this approach provides a rigorous validation of quantum-corrected drift-diffusion solvers that account for TAT by means of a modified LDOS, obtained either from analytical models [12–15,19–21], numerical approximations, e.g., the localization landscape theory [22,23], or directly from the solution of the Schrödinger equation [24].

II. THEORY

Restricting our analysis to steady-state conditions, in which only time differences matter, we can Fourier transform the Green's functions to the energy domain. In layered structures, an additional Fourier transform is performed with respect to the homogeneous transverse coordinates $\underline{r}_{\parallel}$ [25], i.e.,

$$G(\underline{r}, \underline{r}', E) = \mathcal{A}^{-1} \sum_{\underline{k}} G(\underline{k}, z, z', E) e^{i\underline{k} \cdot (\underline{r}_{\parallel} - \underline{r}'_{\parallel})}, \quad (1)$$

where z is the symmetry-broken direction and $\mathcal{A}$ is the normalization area. Having defined G_0^R as the Green's function of the noninteracting system

$$[E - H(\underline{k}, z)] G_0^R(\underline{k}, z, z', E) = \delta(z - z'), \quad (2)$$

where H is the noninteracting Hamiltonian that includes the electronic structure and the electrostatic mean-field potential, the steady-state Dyson and Keldysh equations can be written as [26,27]

$$G^R(\underline{k}, z, z', E) = G_0^R(\underline{k}, z, z', E) + \int dz_1 \int dz_2$$
$$\times G_0^R(\underline{k}, z, z_1, E) \Sigma^R(\underline{k}, z_1, z_2, E)$$
$$\times G^A(\underline{k}, z_2, z', E), \quad (3)$$

$$G^<(\underline{k}, z, z', E) = \int dz_1 \int dz_2 \, G^R(\underline{k}, z, z_1, E)$$
$$\times \Sigma^<(\underline{k}, z_1, z_2, E) G^A(\underline{k}, z_2, z', E). \quad (4)$$

The self-energy Σ includes the boundary self-energy expressing the openness of the system, the carrier-phonon self-energy Σ_{ep}, and an additional (local) self-energy Σ_{SRH}, which describes SRH recombination within the multiphonon defect-scattering scheme proposed in Ref. [18]. The numerical discretization of (3) and (4) is based on a multiband 8×8 $k \cdot p$ description of the electronic structure for wurtzite crystals [28–30], which includes the first conduction band, heavy-hole, light-hole, and spin-orbit split-off bands; see Appendix A.

Interactions with (bulk) phonons are encoded in the self-energy

$$\Sigma_{ep}^{\lessgtr}(\underline{k}, z, z', E) = \sum_{\lambda \underline{Q}} |U_{\lambda \underline{Q}}|^2 e^{iq_z(z-z')}$$
$$\times [N_{\lambda \underline{Q}} \, G^{\lessgtr}(\underline{k} - \underline{q}, z, z', E \mp \hbar\omega_{\lambda\underline{Q}})$$
$$+ (N_{\lambda\underline{Q}} + 1) G^{\lessgtr}(\underline{k} - \underline{q}, z, z', E \pm \hbar\omega_{\lambda\underline{Q}})], \quad (5)$$

where the number of phonons $N_{\lambda Q}$ with wavevector $\underline{Q} = (\underline{q}, q_z)$ in mode λ is given by the Bose-Einstein distribution, the phonon system being supposed to be at equilibrium [31,32]. According to deformation-potential scattering theory, the scattering strength U_Q due to the interaction with acoustic modes is described by

$$U_Q = \sqrt{\frac{\hbar D_a^2}{2\mathcal{V}\rho u_l} Q}, \quad (6)$$

where $u_l = 6.56 \times 10^5$ cm/s is the longitudinal sound velocity in the material, $D_a = 8$ eV [33] is the acoustic deformation potential, $\rho = 6.15$ g/cm^3 is the semiconductor mass density, and $\mathcal{V}$ is the normalization volume. Fröhlich theory of polar optical scattering gives the interaction strength

$$U_Q = \sqrt{\frac{e^2 \hbar \omega_{LO}}{2\mathcal{V}} \left(\frac{1}{\epsilon_\infty} - \frac{1}{\epsilon_s} \right)} \frac{Q}{Q^2 + q_0^2}, \quad (7)$$

where $\epsilon_s = 10$ and $\epsilon_\infty = 5.3$ are the static and optical dielectric permittivities of the material, and q_0 is the

inverse of the Debye-Hückel screening length (10 nm in all the simulations below). A dispersionless longitudinal optical phonon with energy $\hbar\omega_{LO} = 90$ meV has been assumed.

SRH recombination is described within the multiphonon defect-scattering scheme proposed in Ref. [18]. For brevity, we present the theory for electrons in the conduction band interacting for a single defect level with energy E_d, placed at $z = z_0$. Similar expressions hold for the valence band [18]. The generalization to a distribution of defects is straightforward if the defect levels are considered independent from each other (save for the indirect link via the electrostatics), as implied in the conventional SRH theory. In principle, interdefect charge transfer is possible. For example, defect states may act as stepping stones in the *off* state of tunnel-field-effect transistors, while in the *on* state, they can affect the electron transport indirectly by modifying the device electrostatics [34,35]. The possibility of multidefect tunneling through a series of defects can be neglected if the distance between the defects is large compared to typical tunneling paths [36]. This condition applies if the defect density ρ_d is less than, say, 10^{15} cm^{-3}, which corresponds to an average distance between defects of 100 nm. For such low defect densities, the trapped charge, which in principle may screen spontaneous and piezoelectric polarization fields, can be neglected in the self-consistent solution of Poisson's equation.

The (local) self-energies that describe the capture or emission of an electron in the conduction band into or from the defect state are [18]

$$\Sigma_{SRH}^{\lessgtr}(z,z',E) = \rho_d \sum_{l\geq 0} \mathcal{M}_{em/capt}(l)$$
$$\times G_d^{\lessgtr}(E - l\hbar\Omega_0)\delta(z,z_0)\delta(z',z_0), \quad (8)$$

where Ω_0 is the frequency of an effective dispersionless phonon mode, whose energy was chosen to be equal to the polar optical phonon energy in GaN (90 meV). A local quasiequilibrium is assumed for the defect correlation functions

$$G_d^<(E) = if_d(E)A_d(E), \quad (9)$$
$$G_d^>(E) = -i[1 - f_d(E)]A_d(E), \quad (10)$$

where $A_d(E) = 2\pi\delta(E - E_d)$ is the (unscattered) spectral function of the defect. The multiphonon matrix element of the capture process is [18,37]

$$\mathcal{M}_{capt}(l) = \mathcal{M}_{dc}^0 \frac{(l - S)^2}{S}\exp[-S(2f_B + 1)]$$
$$\times \left(\frac{f_B + 1}{f_B}\right)^{l/2} I_l[2S\sqrt{f_B(f_B + 1)}], \quad (11)$$

where $S = 10$ is the Huang-Rhys factor in GaN [8], I_l is the modified Bessel function of order l, and

$f_B = \{\exp[(\hbar\Omega_0/k_BT)] - 1\}^{-1}$ is the Bose-Einstein occupation probability of the vibrational mode. The matrix element of the emission process can be obtained from the detailed balance principle $\mathcal{M}_{em}(l) = \mathcal{M}_{capt}(l)\exp(-\beta l\hbar\Omega_0)$, with $\beta = 1/(k_BT)$. The unknown coupling constant $\mathcal{M}_{dc}^0$ between defect and conduction-band states can be obtained from the experimental capture cross sections, by comparing the bulk SRH rate expression with the corresponding NEGF version in the quasiequilibrium limit, in which the occupations of band and defect states are given by Fermi statistics [18].

The defect occupation function f_d is obtained from [18]

$$\Sigma_d^<(E_d) = if_d(E_d)\Gamma_d(E_d), \quad (12)$$

where $\Gamma_d = i(\Sigma_d^> - \Sigma_d^<)$,

$$\Sigma_d^{\lessgtr}(E) = \mathcal{A}^{-1}\sum_{\underline{k}}\sum_{l\geq 0}\mathcal{M}_{capt/em}(l)$$
$$\times G^{\lessgtr}(\underline{k},z_0,z_0,E + l\hbar\Omega_0). \quad (13)$$

On a quantum-kinetic level, the steady-state conservation laws for charge carrier densities, complemented with Poisson's equation accounting for electron-electron interactions at the Hartree level, are formulated in terms of the carrier Green's functions and self-energies (again we report only the equations for the electrons) [38]:

$$\partial_z^2\phi(z) = -\frac{e}{\epsilon_s}[N_D(z) - N_A(z) + p(z) - n(z)], \quad (14)$$

$$\partial_z J_n(z) = e\,U_n(z), \quad (15)$$

$$n(z) = \mathcal{A}^{-1}\sum_{\underline{k}}\int\frac{dE}{2\pi}[-iG^<(\underline{k},z,z,E)], \quad (16)$$

$$J_n(z) = \mathcal{A}^{-1}\sum_{\underline{k}}\int\frac{dE}{2\pi}\lim_{z'\to z}\frac{e\hbar}{m_0}(\partial_z - \partial_{z'})G^<(\underline{k},z,z',E). \quad (17)$$

Here e is the elementary charge, N_D is the net donor density, n and p are the electron and hole densities, m_0 is the bare electron mass, and U_n is the recombination rate

$$U_n(z) = -\mathcal{A}^{-1}\sum_{\underline{k}}\int\frac{dE}{2\pi\hbar}\int dz'$$
$$\times [\Sigma^R(\underline{k},z,z',E)G^<(\underline{k},z',z,E)$$
$$+ \Sigma^<(\underline{k},z,z',E)G^A(\underline{k},z',z,E)$$
$$- G^R(\underline{k},z,z',E)\Sigma^<(\underline{k},z',z,E)$$
$$- G^<(\underline{k},z,z',E)\Sigma^A(\underline{k},z',z,E)]. \quad (18)$$

Because of the additive property of the self-energies in Eq. (18), we can decompose U_n into the sum of different scattering processes. Upon convergence of the self-consistent Born cycle, the contribution of intraband mechanisms (e.g., the interaction with phonons) should vanish when the integral over energy is performed over one of the two (conduction or valence) bands, while, if the integration is restricted to one of the two bands, the contribution of Σ_{SRH} provides the (net) SRH recombination rate U_{SRH}.

Carrier-carrier interactions on a mean-field level are included in the self-consistent solution of Poisson's equation, Eq. (14), which relates the Hartree electrostatic potential entering the Hamiltonian with the electronic density provided by the Green's function expression, Eq. (16). In practice, two nested loops are needed for the calculation of the Green's functions: an inner loop to achieve self-consistency between Green's functions and self-energies, and an outer loop to update the electrostatic potential [25].

III. RESULTS

The structure under consideration is a single-quantum-well LED (device A2 in Ref. [7]), which includes an n-doped GaN buffer layer ($N_D = 1 \times 10^{20}$ cm^{-3}), a 4 nm GaN spacer (SP), a 3 nm In$_{0.17}$Ga$_{0.83}$N quantum well (QW), a 4 nm quantum barrier (QB), a 20 nm p-doped Al$_{0.13}$Ga$_{0.87}$N electron-blocking layer (EBL) with $N_A = 5 \times 10^{19}$ cm^{-3} and a p-GaN contact region with the same doping concentration. Incomplete dopant ionization is assumed, with activation energies $\Delta E_D = 20$ meV and $\Delta E_A = 200$ meV for donors and acceptors, respectively. Spontaneous and piezoelectric charges at heterointerfaces are determined according to the model proposed by Bernardini and Fiorentini (BF) [39]. The conduction-band-edge discontinuity is set to 70% of the energy gap. A combined capacitance-voltage and steady-state photocapacitance study of defect incorporation in GaN-based LEDs indicates that the defects are located near midgap, and that their density peaks in In$_x$Ga$_{1-x}$N layers, with some spreading in the surrounding regions, which was attributed to the surface segregation of In atoms [40]. For simplicity, we assume a uniform distribution of traps located at midgap. In all simulations, uniform grid spacings are used in energy and momentum space, with values $\Delta E = 5$ meV and $\Delta k = 5$ nm^{-1}, respectively. The device region is discretized with a grid step of 0.5 nm along the growth direction. Figure 1 shows the LDOS (color maps), i.e., the diagonal elements of the spectral function $A = i(G^R - G^A)$, evaluated at $\underline{k} = 0$ for a forward bias of 2 V. The green line represents the position of the trap level. Shades of blue in the LDOS mark the position of (quasi)bound states in the QW. The black contour lines of the LDOS indicate a decrease of 2 orders of magnitude in the tail states (not visible in a linear color map) away
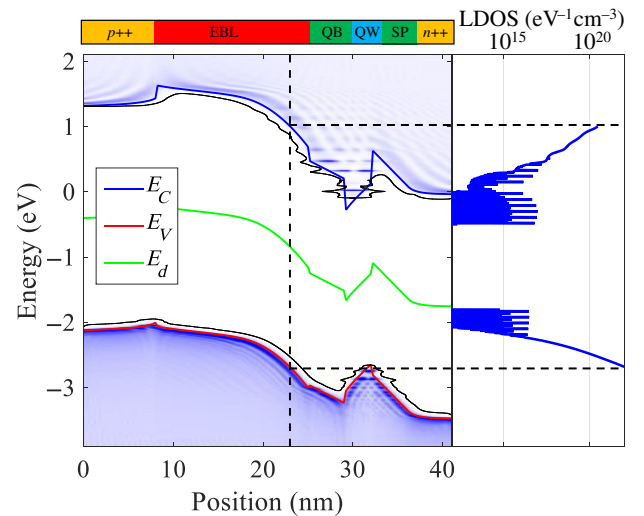

FIG. 1.   Local density of states (left panel, color maps) of a single-quantum-well LED in weak forward bias, showing a complex structure of bound and quasibound states. Contour lines (black curves) show the extension of these resonant states in the energy gap. The green line marks the energy level of the defect, which is assumed to be at midgap (conduction and valence edges are represented by blue and red lines, respectively) and uniformly distributed in the structure. Sharp phonon resonances related to multiphonon relaxation can be observed in the logarithmic plot of the LDOS evaluated at $z = 23$ nm (right panel), where U_{SRH} is maximum.

from the band edges. The LDOS evaluated near the EBL-QB heterointerface, where U_{SRH} peaks, is shown in the right panel of Fig. 1 (blue lines). Superimposed to the resonances due to confined states extending in the energy gap, sharp phonon resonances related to multiphonon relaxation can be clearly observed in the tails of the LDOS.

In the high-electric-field region where most of the recombination occurs, the contribution of carrier-phonon scattering to the formation of the tail states is negligible with respect to the field-induced contribution; the Urbach tails due to deformation potential and polar optical scattering can be better appreciated in the flat-band regions (the quasineutral layers of the LED), where the subgap states induced by the band bending are not present. A detailed discussion on band-tail formation and band-gap narrowing due to polar optical phonon and impurity scattering within a NEGF framework can be found in Ref. [16]. Therefore, we may argue that the tunneling assisting SRH recombination is mainly a coherent process. However, as already observed in the case of BTBT [32], inelastic carrier-phonon scattering is responsible for the population of the confined states in the QW, which cannot be reached directly from the contacts, and thus indirectly contributes to TAT.
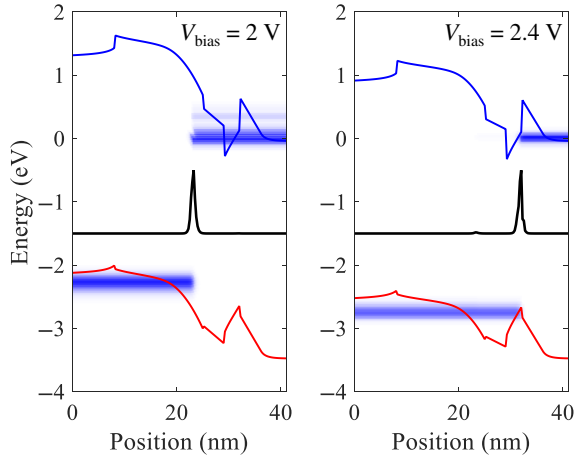
FIG. 2. SRH scattering current computed with NEGF at a forward bias of 2 V (left panel) and 2.4 V (right panel). The continuous stripes, corresponding to current-carrying channels, switch bands where U_{SRH} is maximum. Black lines represent the corresponding energy-integrated recombination rates (arbitrary units). All simulations are performed at room temperature. The total energy-integrated currents are perfectly conserved.
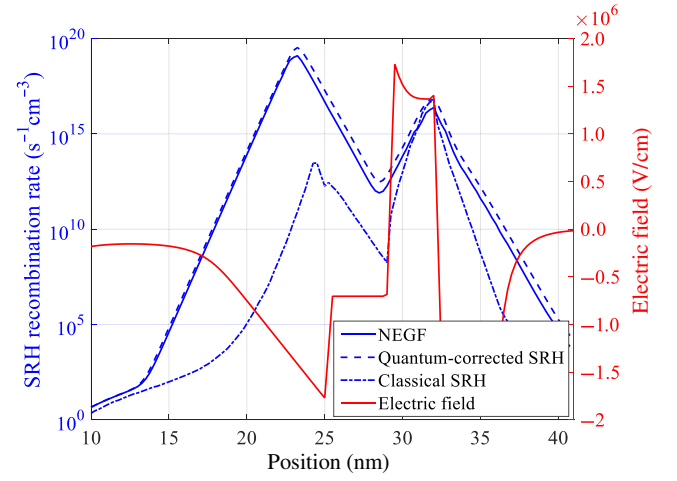

FIG. 3. SRH recombination rates computed with different models at a forward bias of 2 V (blue lines, left axis), and the electric field profile (red line, right axis). The SRH rate computed with NEGF (solid blue line) is well reproduced by the quantum-corrected SRH rate (dashed blue line) computed from Eq. (20) with the NEGF carrier densities. Neglecting tail states, which corresponds to the classical limit (i.e., SRH without the inclusion of tunneling), significantly underestimates the recombination rate (dotted blue line).

The SRH scattering current can be computed as

$$J_{SRH}(z, E) = e \int_{-\infty}^{z} dz' \, U_{SRH}(z', E), \tag{19}$$

where the spectral recombination rate $U_{SRH}(z, E)$ is obtained from Eq. (18), ignoring the integral over energy [41]. The resulting spectral current for different forward biases is shown in Fig. 2. Current-carrying channels (continuous horizontal stripes originating from the contacts), fade away when they reach the region where U_{SRH} (solid black line) is nonzero. The position of the recombination window is the result of a complex interplay between tunneling probabilities and multiphonon matrix elements. At a bias of 2 V, most of the recombination occurs near the EBL-QB heterojunction, where the magnitude of the electric field is maximum (red line in Fig. 3). The electrons reach the EBL by resonant tunneling (the electron spectral current approximately flows at the ground state energy of the QW), while holes have to tunnel a shorter distance before reaching the virtual states that participate in the recombination process. A logarithmic plot of the SRH rate at 2 V (solid blue line in Fig. 3) reveals a second smaller peak in the QW, not visible in a linear scale. This second peak gradually increases with the applied bias, moving the recombination window towards the n side of the junction at 2.4 V. Looking at the carrier densities as a function of the applied bias in Fig. 4, we can see that the shift in the recombination window may be traced back to the slow increase in the hole population in the QW. The different bias dependencies of electron and hole populations in the QW is indicative of inefficient hole injection, which has been

reported as the origin of the inhomogeneous distribution of holes in multi-QW LEDs [42].

SRH theory in NEGF was proven to be equivalent, in a bulk semiconductor, to the conventional semiclassical SRH formula [18]

$$U_{SRH}(z) = \frac{np - n_{eq}p_{eq}}{\tau_p(n + n_1) + \tau_n(p + p_1)}, \tag{20}$$

where n_{eq}, p_{eq} are the electron and hole densities at equilibrium, n_1, p_1 are the corresponding quantities when the
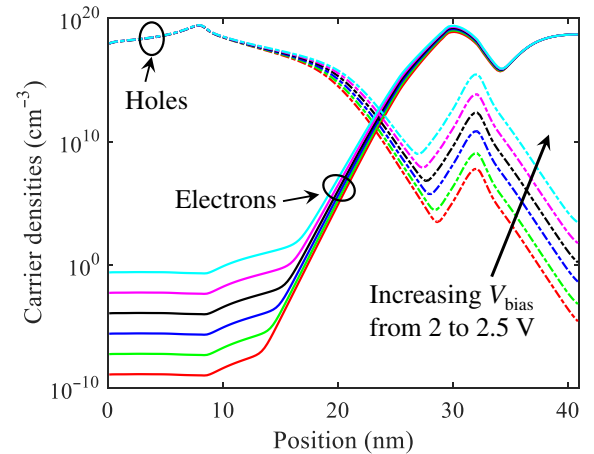

FIG. 4. Electron and hole densities at different forward bias voltages.

Fermi level falls at the trap energy level, and τ_n, τ_p are the electron and hole lifetimes corresponding to the constants $\mathcal{M}_{dc}^0$ and $\mathcal{M}_{dv}^0$, coupling the defect with the conduction (dc) and valence (dv) bands, respectively; see [18, Appendix B] for the connection between multiphonon matrix elements and trap cross sections. Equation (20) can be formally recovered from Eq. (18) only in quasiequilibrium conditions, i.e., when correlation and spectral functions are related by a *local* fluctuation-dissipation relation [18]. It is interesting to see whether Eq. (20), with the correct quantum carrier densities, can still reproduce the field-enhanced SRH rate in a nanostructure. The SRH rate obtained from Eq. (20) using the carrier densities computed with NEGF is shown in Fig. 3 (dashed blue line). The good agreement with NEGF calculations suggests that drift-diffusion solvers with a quantum-corrected LDOS obtained, e.g., from the self-consistent solution of the Schrödinger equation [24] or the localization landscape theory [23], represent a viable approach to the analysis of TAT. Indeed, within these quantum-corrected DD schemes, TAT would be naturally included within the standard SRH theory, without the need of specific models for field enhancement factors, whose expressions tend to be overly complex, with many unknown quantities, in particular the tunneling masses, treated as fitting parameters [8].

Finally, Fig. 5 shows the *I-V* characteristics of the LED computed with the NEGF approach (blue line) and from experiments (blue circles). The fitting of the experimental results is obtained by assuming that $\tau_n = \tau_p = 1$ ns, which is compatible with defect concentrations and cross sections reported in Ref. [7]. In the subthreshold regime, below the

optical turn on, TAT is the most relevant contribution to carrier transport. Deviations from the ideal behavior predicted by Shockley theory can be better appreciated by looking at the ideality factor [8]

$$\eta = \frac{q}{k_B T} \frac{\partial V}{\partial [\ln I]}, \tag{21}$$

shown in Fig. 5 (red line and circles). Ideality factors between one and two are normally attributed to the competition between diffusion and the recombination processes, while ideality factors exceeding two are attributed to tunneling. For bias voltages above 2.5 V, as the diffusion current (dashed blue line) becomes dominant, η decreases, approaching one, before increasing again due to the resistive behavior of the diode.

IV. CONCLUSION

In this work we present a NEGF study of TAT in GaN-based LEDs. The computed ideality factors are in agreement with experiments. We also show that the standard SRH formula, computed with the correct quantum carrier densities, can reproduce NEGF results. Carrier densities may be estimated, e.g., from localization landscape approaches [23], or more rigorously from the full eigendecomposition of the Schrödinger equation. Among possible quantum-corrected semiclassical approaches to study carrier transport in LEDs, the Schrödinger-Poisson drift-diffusion model [24] seems promising. DD models, complemented with a quantum-corrected LDOS, may be the only viable approach to the numerical simulation of complex realistic structures. For example, disorder effects call for full three-dimensional LED simulations [42], which are beyond the grasp of NEGF approaches. Additional work is needed to verify the accuracy of such quantum-corrected semiclassical models, especially in the high-injection regime, where out-of-equilibrium phenomena such as hot carrier transport become relevant.
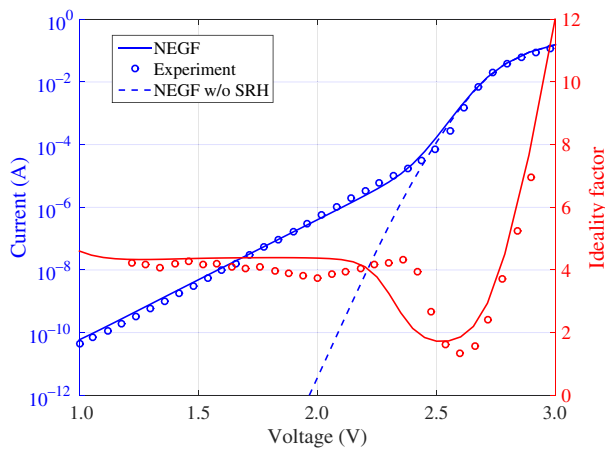

FIG. 5. The *I-V* characteristics (left axis) and corresponding ideality factor (right axis), computed with the NEGF approach (solid lines) and from measurements [7] (circles). A series resistance $R_s = 1\Omega$, accounting for nonideal contacts and buffer layers, is selected to match the slope of the experimental *I-V* curve at high voltages.

APPENDIX: NUMERICAL DISCRETIZATION

The starting point for the numerical discretization of the NEGF equations is the eight-band $k \cdot p$ bulk Hamiltonian for (0001)-oriented wurtzite semiconductors [30]

$$H_{k \cdot p} = \begin{bmatrix} E_c & 0 & -(k_+P_2)/\sqrt{2} & (k_-P_2)/\sqrt{2} & k_zP_1 & 0 & 0 & 0 \\ 0 & E_c & 0 & 0 & 0 & (k_-P_2)/\sqrt{2} & -(k_+P_2)/\sqrt{2} & k_zP_1 \\ -P_2k_-/\sqrt{2} & 0 & F & -(K^\dagger)^* & -(H_+^\dagger)^* & 0 & 0 & 0 \\ P_2k_+/\sqrt{2} & 0 & -K^* & G & H_-^\dagger & 0 & 0 & \sqrt{2}\Delta_3 \\ P_1k_z & 0 & -H_+^* & H_- & \Lambda & 0 & \sqrt{2}\Delta_3 & 0 \\ 0 & P_2k_+/\sqrt{2} & 0 & 0 & 0 & F^* & -K^* & H_-^\dagger \\ 0 & -P_2k_-/\sqrt{2} & 0 & 0 & \sqrt{2}\Delta_3 & -(K^\dagger)^* & G^* & -(H_+^\dagger)^* \\ 0 & P_1k_z & 0 & \sqrt{2}\Delta_3 & 0 & H_- & -H_+^* & \Lambda \end{bmatrix},$$

$$\text{(A1)}$$

written in the zone-center basis

$$|1\rangle = |iS\uparrow\rangle, \qquad |2\rangle = |iS\downarrow\rangle,$$

$$|3\rangle = \left| -\frac{1}{\sqrt{2}}(X + iY)\uparrow \right\rangle, \qquad |4\rangle = \left| \frac{1}{\sqrt{2}}(X - iY)\uparrow \right\rangle, |5\rangle = |Z\uparrow\rangle,$$

$$|6\rangle = \left| \frac{1}{\sqrt{2}}(X - iY)\downarrow \right\rangle, \qquad |7\rangle = \left| -\frac{1}{\sqrt{2}}(X + iY)\downarrow \right\rangle, |8\rangle = |Z\downarrow\rangle,$$

with

$$k_\pm = k_x \pm ik_y,$$

$$E_c = E_g + \Delta_1 + \Delta_2 + \frac{\hbar^2}{2m_0}[k_xA_tk_x + k_yA_tk_y + k_zA_zk_z], \tag{A2}$$

$$\Lambda = \frac{\hbar^2}{2m_0}[k_zA_1k_z + k_xA_2k_x + k_yA_2k_y], \tag{A3}$$

$$\Theta = \frac{\hbar^2}{2m_0}[k_zA_3k_z + k_xA_4k_x + k_yA_4k_y], \tag{A4}$$

$$F = \Delta_1 + \Delta_2 + \Lambda + \Theta$$
$$+ \frac{\hbar^2}{2m_0}[-ik_y(A_5^+ - A_5^-)k_x + ik_x(A_5^+ - A_5^-)k_y], \tag{A5}$$

$$G = \Delta_1 - \Delta_2 + \Lambda + \Theta$$
$$+ \frac{\hbar^2}{2m_0}[-ik_x(A_5^+ - A_5^-)k_y + ik_y(A_5^+ - A_5^-)k_x], \tag{A6}$$

$$K = \frac{\hbar^2}{2m_0}[k_xA_5k_x - i(k_xA_5k_y + k_xA_5k_y) - k_yA_5k_y], \tag{A7}$$

$$H_\pm = \frac{\hbar^2}{2m_0}[k_zA_6^+(k_x - ik_y) + (k_x - ik_y)A_6^-k_z]$$
$$\pm iA_7(k_x - ik_y). \tag{A8}$$

Here $\Delta_1 = \Delta_{\text{cr}}$ is the crystal field splitting energy and $\Delta_2 = \Delta_3 = \Delta_{\text{SO}}/3$ with Δ_{SO} the spin-orbit splitting

energy. The notation introduced by Veprek [29] has been used to indicate operator ordering, needed for numerical stability. The $k \cdot p$ band parameters are taken from Ref. [43]. By using the basis transformation $H'_{k \cdot p} = T^*H_{k \cdot p}T^T$, with

$$T = \begin{bmatrix} i\beta^* & \alpha & 0 & 0 & 0 & 0 & 0 & 0 \\ 0 & 0 & \alpha^* & 0 & 0 & \alpha & 0 & 0 \\ 0 & 0 & 0 & \beta & 0 & 0 & \beta^* & 0 \\ 0 & 0 & 0 & 0 & \beta^* & 0 & 0 & \beta \\ i\beta^* & -\alpha & 0 & 0 & 0 & 0 & 0 & 0 \\ 0 & 0 & \alpha^* & 0 & 0 & -\alpha & 0 & 0 \\ 0 & 0 & 0 & \beta & 0 & 0 & -\beta^* & 0 \\ 0 & 0 & 0 & 0 & -\beta^* & 0 & 0 & \beta \end{bmatrix},$$

where $\alpha = e^{i(3\pi/4 + 3\phi/2)}/\sqrt{2}$, $\beta = e^{i(\pi/4 + \phi/2)}/\sqrt{2}$, and $\phi = \text{atan}(k_y/k_x)$, the bulk 8×8 Hamiltonian (A1) is block diagonalized with respect to the spin components into two (real) 4×4 blocks, which simplifies the numerical evaluation of the Green's functions. Within a finite-element scheme and the envelope function approximation, the basis functions include plane waves in the transverse direction $\underline{r}_\parallel$, tent-shaped functions $t_i(z)$ peaked at z_i, and zone-centre lattice-periodic functions $u_a(\underline{r})$:

$$\phi_{\underline{k}\alpha} = \frac{1}{\sqrt{\mathcal{A}}}t_i(z)e^{i\underline{k}\cdot\underline{r}_\parallel}u_a(\underline{r}). \tag{A9}$$

Here $\alpha = (a, i)$ is a compound index combining indices a for band and i for space.

Since the finite-element basis functions $\{t_i(z)\}$ are not orthogonal, a mixed representation is needed for Green's

functions and self-energies [44]. Using a contravariant representation for Green's functions,

$$G(\underline{k}, z, z', E) = \sum_{\alpha\beta} \phi_{\underline{k}\alpha}(\underline{r}) G_{\alpha\beta}(\underline{k}, E) \phi_{\underline{k}\beta}^*(\underline{r}'), \qquad (A10)$$

and a covariant representation for self-energies,

$$\Sigma_{\alpha\beta}(\underline{k}, E) = \int d\underline{r} d\underline{r}' \phi_{\underline{k}\alpha}^*(\underline{r}) \Sigma(\underline{k}, z, z', E) \phi_{\underline{k}\beta}(\underline{r}'), \quad (A11)$$

the basis-transformed versions of Eqs. (3) and (4) read, in full matrix notation [27,45,46],

$$[E\mathbf{M} - \mathbf{H}(\underline{k}) - \mathbf{\Sigma}^R(\underline{k}, E)]\mathbf{G}^R(\underline{k}, E) = I, \qquad (A12)$$

$$\mathbf{G}^{\lessgtr}(\underline{k}, E) = \mathbf{G}^R(\underline{k}, E)\mathbf{\Sigma}^{\lessgtr}(\underline{k}, E)\mathbf{G}^A(\underline{k}, E), \qquad (A13)$$

where $\mathbf{G}$ and $\mathbf{\Sigma}$ are matrices that depend parametrically on $\underline{k}$ and E, with dimensions equal to the number of bands times the number of spatial grid points in the symmetry-broken direction z, and $\mathbf{M}$ is the (nondiagonal) overlap matrix

$$M_{\alpha\beta} = \int d\underline{r} \phi_{\underline{k}\alpha}^*(\underline{r}) \phi_{\underline{k}\beta}^*(\underline{r}) \approx \delta_{ab} \int dz\, t_i(z) t_j(z) \qquad (A14)$$

with $\alpha = (a, i)$ and $\beta = (b, j)$. The last approximation is afforded by the coarse-graining assumption of $k\cdot p$ theory [45,47]. Additional details concerning the finite-element dicretization procedure and the implementation of the boundary self-energies can be found in Refs. [31,32].

---

[1] N. I. Bochkareva, V. V. Voronenkov, R. I. Gorbunov, A. S. Zubrilov, Y. S. Lelikov, P. E. Latyshev, Y. T. Rebane, A. I. Tsyuk, and Y. G. Shreter, Defect-related tunneling mechanism of efficiency droop in III-nitride light-emitting diodes, Appl. Phys. Lett. **96**, 133502 (2010).

[2] G. Verzellesi, D. Saguatti, M. Meneghini, F. Bertazzi, M. Goano, G. Meneghesso, and E. Zanoni, Efficiency droop in InGaN/GaN blue light-emitting diodes: Physical mechanisms and remedies, J. Appl. Phys. **114**, 071101 (2013).

[3] J. Hader, J. V. Moloney, and S. W. Koch, Density-activated defect recombination as a possible explanation for the efficiency droop in GaN-based diodes, Appl. Phys. Lett. **96**, 221106 (2010).

[4] A. David, N. G. Young, C. A. Hurni, and M. D. Craven, Quantum Efficiency of III-Nitride Emitters: Evidence for Defect-Assisted Nonradiative Recombination and its Effect on the Green gap, Phys. Rev. Appl. **11**, 031001 (2019).

[5] A. C. Espenlaub, D. J. Myers, E. C. Young, S. Marcinkevicius, C. Weisbuch, and J. S. Speck, Evidence of trap-assisted Auger recombination in low radiative efficiency MBE-grown III-nitride LEDs, J. Appl. Phys. **126**, 184502 (2019).

[6] A. David, N. G. Young, C. Lund, and M. D. Craven, Review–the physics of recombinations in III-nitride emitters, ECS J. Solid State Sci. Technol. **9**, 016021 (2020).

[7] M. Auf der Maur, B. Galler, I. Pietzonka, M. Strassburg, H. Lugauer, and A. Di Carlo, Trap-assisted tunneling in InGaN/GaN single-quantum-well light-emitting diodes, Appl. Phys. Lett. **105**, 133504 (2014).

[8] M. Mandurrino, G. Verzellesi, M. Goano, M. Vallone, F. Bertazzi, G. Ghione, M. Meneghini, G. Meneghesso, and E. Zanoni, Physics-based modeling and experimental implications of trap-assisted tunneling in InGaN/GaN light-emitting diodes, Phys. Status Solidi A **212**, 947 (2015).

[9] M. Goano, F. Bertazzi, X. Zhou, M. Mandurrino, S. Dominici, M. Vallone, G. Ghione, A. Tibaldi, M. Calciati, P. Debernardi, F. Dolcini, F. Rossi, G. Verzellesi, M. Meneghini, N. Trivellin, C. De Santi, E. Zanoni, and E. Bellotti, Challenges towards the simulation of GaN-based LEDs beyond the semiclassical framework, in *SPIE Photonics West, Physics and Simulation of Optoelectronic Devices XXIV*, B. Witzigmann, M. Osiński, and Y. Arakawa, Eds., vol. 9742, Proceedings of the SPIE, San Francisco, CA, Feb. 2016, p. 974202.

[10] C. De Santi, M. Buffolo, N. Renso, A. Neviani, G. Meneghesso, E. Zanoni, and M. Meneghini, Evidence for defect-assisted tunneling and recombination at extremely low current in InGaN/GaN-based LEDs, Appl. Phys. Express **12**, 052007 (2019).

[11] M. Meneghini, C. De Santi, A. Tibaldi, M. Vallone, F. Bertazzi, G. Meneghesso, E. Zanoni, and M. Goano, Thermal droop in III-nitride based light-emitting diodes: Physical origin and perspectives, J. Appl. Phys. **127**, 211102 (2020).

[12] G. A. M. Hurkx, D. B. M. Klaassen, and M. P. G. Knuvers, A new recombination model for device simulation including tunneling, IEEE Trans. Electron Devices **39**, 331 (1992).

[13] A. Schenk, An improved approach to the Shockley-Read-Hall recombination in inhomogeneous fields of space-charge regions, J. Appl. Phys. **71**, 3339 (1992).

[14] A. Schenk, A model for the field and temperature dependence of Shockley-Read-Hall lifetimes in silicon, Solid-State Electron. **35**, 1585 (1992).

[15] X. Gao, B. Kerr, and A. Huang, Analytic band-to-trap tunneling model including band offset for heterojunction devices, J. Appl. Phys. **125**, 054503 (2019).

[16] P. Sarangapani, Y. Chu, J. Charles, G. Klimeck, and T. Kubis, Band-Tail Formation and Band-Gap Narrowing Driven by Polar Optical Phonons and Charged Impurities in Atomically Resolved III-V Semiconductors and Nanodevices, Phys. Rev. Appl. **12**, 044045 (2019).

[17] S. Sant and A. Schenk, The effect of density-of-state tails on band-to-band tunneling: theory and application to tunnel field effect transistors, J. Appl. Phys. **122**, 135702 (2017).

[18] U. Aeberhard, Nonequilibrium Green's function picture of nonradiative recombination of the Shockley-Read-Hall type, Phys. Rev. B **99**, 125302 (2019).

[19] T. Höhr, A. Schenk, and W. Fichtner, Revised Shockley-Read-Hall lifetimes for quantum transport modeling, J. Appl. Phys. **95**, 4875 (2004).

[20] M. Baudrit and C. Algora, Tunnel diode modeling, including nonlocal trap-assisted tunneling: a focus on III–V

multijunction solar cell simulation, IEEE Trans. Electron Devices **57,** 2564 (2010).

[21] A. Schenk and S. Sant, tunneling between density-of-state tails: Theory and effect on Esaki diodes, J. Appl. Phys. **128,** 014502 (2020).

[22] D. N. Arnold, G. David, D. Jerison, S. Mayboroda, and M. Filoche, Effective Confining Potential of Quantum States in Disordered Media, Phys. Rev. Lett. **116,** 056602 (2016).

[23] M. Filoche, M. Piccardo, Y. Wu, C. Li, C. Weisbuch, and S. Mayboroda, Localization landscape theory of disorder in semiconductors. I. Theory and modeling, Phys. Rev. B **95,** 144204 (2017).

[24] C. de Falco, E. Gatti, A. L. Lacaita, and R. Sacco, Quantum-corrected drift-diffusion models for transport in semiconductor devices, J. Comp. Phys. **204,** 533 (2005).

[25] U. Aeberhard, Photovoltaics at the mesoscale: insights from quantum-kinetic simulation, J. Phys. D **51,** 323002 (2018).

[26] U. Aeberhard and R. H. Morf, Microscopic nonequilibrium theory of quantum well solar cells, Phys. Rev. B **77,** 125343 (2008).

[27] F. Bertazzi, M. Goano, G. Ghione, A. Tibaldi, P. Debernardi, and E. Bellotti, Electron transport, in *Handbook of Optoelectronic Device Modeling and Simulation*, J. Piprek, Ed. Boca Raton, FL: CRC Press, 2017, ch. 2, pp. 35–80.

[28] S. L. Chuang and C. S. Chang, $k \cdot p$ method for strained wurtzite semiconductors, Phys. Rev. B **54,** 2491 (1996).

[29] R. G. Veprek, S. Steiger, and B. Witzigmann, Operator ordering, ellipticity and spurious solutions in $k \cdot p$ calculations of III-nitride nanostructures, Opt. Quantum Electron. **40,** 1169 (2008).

[30] X. Zhou, F. Bertazzi, M. Goano, G. Ghione, and E. Bellotti, Deriving $k \cdot p$ parameters from full-brillouin-zone descriptions: a finite-element envelope function model for quantum-confined wurtzite nanostructures, J. Appl. Phys. **116,** 033709 (2014).

[31] F. Bertazzi, A. Tibaldi, M. Goano, J. A. Gonzalez Montoya, and E. Bellotti, Nonequilibrium Green's Function Modeling of type-II Superlattice Detectors and its Connection to Semiclassical Approaches, Phys. Rev. Appl. **14,** 014083 (2020).

[32] A. Tibaldi, J. A. Gonzalez Montoya, M. G. C. Alasio, A. Gullino, A. Larsson, P. Debernardi, M. Goano, M. Vallone, G. Ghione, E. Bellotti, and F. Bertazzi, Analysis of Carrier Transport in Tunnel-Junction Vertical-Cavity Surface-Emitting Lasers by a Coupled Nonequilibrium Green's Function–drift-Diffusion Approach, Phys. Rev. Appl. **14,** 024037 (2020).

[33] F. Bertazzi, M. Moresco, and E. Bellotti, Theory of high field carrier transport and impact ionization in wurtzite

GaN. Part I: A full band Monte Carlo model, J. Appl. Phys. **106,** 063718 (2009).

[34] M. G. Pala, C. Grillet, J. Cao, D. Logoteta, A. Cresti, and D. Esseni, Impact of inelastic phonon scattering in the OFF state of tunnel-field-effect transistors, J. Comp. Electron. **15,** 1240 (2016).

[35] D. Esseni, M. Pala, P. Palestri, C. Alper, and T. Rollo, A review of selected topics in physics based modeling for tunnel field-effect transistors, Semiconductor Sci. Technol. **32,** 083005 (2017).

[36] K. Jandieri, S. D. Baranovskii, O. Rubel, W. Stolz, F. Gebhard, W. Guter, M. Hermle, and A. W. Bett, Resonant electron tunneling through defects in GaAs tunnel diodes, J. Appl. Phys. **104,** 094506 (2008).

[37] B. Das, I. Aguilera, U. Rau, and T. Kirchartz, What is a deep defect? combining Shockley-Read-Hall statistics with multiphonon recombination theory, Phys. Rev. Mater. **4,** 024602 (2020).

[38] U. Aeberhard, Quantum-kinetic theory of photocurrent generation via direct and phonon-mediated optical transitions, Phys. Rev. B **84,** 035454 (2011).

[39] F. Bernardini, in *Nitride Semiconductor Devices: Principles and Simulation*, J. Piprek, Ed. Weinheim: Wiley-VCH Verlag, 2007, ch. 3, p. 49.

[40] F. Piva, C. De Santi, A. Caria, C. Haller, J. F. Carlin, M. Mosca, G. Meneghesso, E. Zanoni, N. Grandjean, and M. Meneghini, Defect incorporation in In-containing layers and quantum wells: Experimental analysis via deep level profiling and optical spectroscopy, J. Phys. D **54,** 025108 (2021).

[41] T. Schmielau, M. F. Pereira, Jr., Nonequilibrium many body theory for quantum transport in terahertz quantum cascade lasers, Appl. Phys. Lett. **95,** 231111 (2009).

[42] C. Weisbuch, S. Nakamura, Y. Wu, and J. S. Speck, Disorder effects in nitride semiconductors: Impact on fundamental and device properties, Nanophoton **10,** 3 (2021).

[43] P. Rinke, M. Winkelnkemper, A. Qteish, D. Bimberg, J. Neugebauer, and M. Scheffler, Consistent set of band parameters for the group-III nitrides AlN, GaN, and InN, Phys. Rev. B **77,** 075202 (2008).

[44] R. K. Lake and R. R. Pandey, Non-equilibrium Green functions in electronic device modeling, https://arxiv.org/abs/cond-mat/0607219, 2006.

[45] S. Steiger, Modelling nano-LEDs, Ph.D. dissertation, Eidgenössische Technische Hochschule Zürich, 2009.

[46] U. Aeberhard, A microscopic theory of quantum well photovoltaics, Ph.D. dissertation, Eidgenössische Technische Hochschule Zürich, 2008.

[47] J. M. Miloszewski and M. S. Wartak, Semiconductor laser simulations using non-equilibrium Green's functions, J. Appl. Phys. **111,** 053104 (2012).